International Journal of Science and Research (IJSR)
ISSN: 2319-7064
SJIF (2022): 7.942

Innovative 3D-Printed Tools Revolutionizing Composite Non-destructive Testing Manufacturing

Kuldeep Sharma[1], Ashok Kumar[2]

NDT Expert
+1501-516-1882
Email: ksmb3112[at]gmail.com

[2]Welding Specialist Welspun
Email: *ashokkumarhbirthl[at]gmail.com*

Abstract: ***In this study, a brand-new framework for designing hybrid additive manufacturing (AM) for making carbon fibre-reinforced plastic hybrids is shown. The feasibility of a concept for an AM structure was assessed by testing its efficacy in terms of mathematical correctness and temperature receptiveness, as well as by modelling the strength unique to each of the thirty distinct AM tools that were meticulously designed and manufactured. The narrow lamination face sheet that was strengthened by the minimum-density mesh architecture made up the AM elements of NDT. Tiny composite parts were laid up and cured satisfactorily using these instruments. When contrasted with comparable bulk monolith instruments, the tooling's temperature responsiveness was up to 17% quicker, attaining over 93% of the given oven warming speed. The findings show that although the temperature rise was more responsive to the face sheet depth, heat overrun was more dependent on the mesh concentration in NDT. The best total morphology was a scaled gyroid mesh with smaller walls at the bottom and thicker walls on the surface, linked to a 0.7 mm solid face sheet. Mesh concentrations as low as 5% were produced. With innovative, lighter, and more environmentally friendly tooling, the study's findings may open up new possibilities for the creation and production of mould instruments, which might have a major effect on the materials sector.***

Keywords: Thermal efficiency · Lattice structures · Composite tooling · Heating rate · Additive manufacturing,Non-destructive Testing (NDT)

1. Introduction

Throughout several industrial areas, the usage of additive manufacturing (AM) technology used NDT is expanding significantly. The liberties offered by this layer-wise producing method permit for greater detail, as shown by the increasing levels of component intricacy in, for example, medical equipment [1-3], heating elements [4-6], and aerospace components and tooling [8–10]. Furthermore, because only necessary substances are used in the disposal process, trash is greatly reduced in NDT. For instance, it has been demonstrated that using AM for component reduction improves assembly life by more than 200% and saves 30% of the substance [11]. Furthermore, life cycle assessment systems have demonstrated a potential decrease of up to 200 million emissions overall by using AM lightweight aeroplane composition, resulting in tonnes of CO2 emissions by the year 2050 [12]. These AM applications of NDT have a lot of promise to increase production effectiveness and conserve energy, especially when construction capacity skills are rising [13]. In addition to the main applications of AM technology, aspects of AM are also used more frequently as supplementary methods of production of NDT. For instance, in moulding, AM is employed in the creation of sand, dies, and expenditure cast moulds. One instance of this from recently is "Enable Casting" [14], which employs customary moulding techniques but with AM-designed and fabricated moulds. This strategy implies that much greater Part difficulty levels can be attained when approaching bulk men. Of the different types of AM techniques and procedures that can be broadly grouped into [15], powder bed fusion (PBF) is the most well-known and commercially important. Several industries are using these AM gadgets, such as thermoforming, moulding by injection, and mould device innovation [16]. The latter is expanding and changing all the time [17–19]. The rising rate of complexity of the items, quickly shortened layout timelines, and rising productivity demands offer substantial opportunities and advantages for the mixtures sector. This, together with the constant reduction of greenhouse gas emissions in accordance with the government's goal of emissions being net-zero and 60% by 2030, has generated a great deal of attention by 2050 [20].The creation and production of equipment of NDT and instruments for blend healing have remained unchanged since the 1970s, when outstanding durability mixtures were first used in aerospace projects. The great majority of mould cutters are produced from single, massive metal billets, usually made of Inconel, stainless steel of NDT, or Invar, and this results in a significant amount of byproduct in the form of debris [21]. Moreover, it takes a lot of power to warm and sustain huge monolithic steel pieces, and doing so can cause unequal temperature gradients throughout the curing period [22]. Large quantities of power are lost when using conventional machining methods in conjunction with the air convection's comparatively poor heat conveyance performance in furnaces and autoclaves [23]. In the course of curing, there are a pair of direct chances to save power: first, by decreasing the weight of the tools and equipment, and second, by boosting process heat transmission. Currently, 15% of the overall electrical output used in the entire lifespan of a conventional fibre-reinforced mixed product can be attributed to the steam curing procedure [24]. Furthermore, while using lighter mixtures instead of steel in the automotive sector lowers pollutants during usage, the environmental effect of producing carbon fibre-reinforced polymers (CFRP) outweighs these power savings [25]. Thus, by concentrating on the mould device's layout, an instant

Licensed Under Creative Commons Attribution CC BY

improvement in efficiency and a decrease in overall embodied power can be attained. Including lightweight components in the machining could be one way to enhance heat response and heat transmission. By lowering the total mass while keeping the necessary total rigidity, these frameworks would produce geometric characteristics with a greater particular rigidity of NDT. In order to improve thermal transfer, lattice frameworks are currently employed in a number of applications, including tube circulation and heat converters [26, 27]. Additionally, metallic bubbles have been proven to accelerate the speed of heat transfer [28, 29], particularly in greater porosity foams where convective heat transfer has been observed to rise by as much as ten times of NDT. Major device weight decreases made possible by AM techniques contribute to increased heat exchange speeds and total temperature awareness of machinery. Therefore, the likelihood of L-PBF producing thermally sensitive machining is highlighted by the effectiveness of lighter lattice frameworks in improving heat transfer efficiency [30].The production of various machinery for the moulding and fixing of various materials is becoming more and more dependent on additive manufacturing of NDT [31–39]. Most of the instances that are now available employ polymer AM methods, like fusion deposition modelling (FDM), to create the tools [18, 40–44]. Huge to near-net form mould devices are made at the Oak Ridge National Laboratory using a Metal Huge Region Additive Manufacturing (AM) method that is being tested [17, 19]. The equipment uses inexpensive metal wire of NDT. Parts with near-net shapes need to undergo extensive afterwards or extra exterior coating procedures. At the moment, only 2.5D flat characteristics are available as geometrical characteristics of NDT. An additional technique for employing carbon fibre-packed ABS thermoplastic as the mould equipment with an exterior coating was tested to demonstrate the viability of the instruments in order to obtain even more customization and more durable composite products [45]. The big CFP parts have been effectively fixed at 180 °C and 620 kPa in an isolator [46]. Nevertheless, little study has been done on the application of completely metallic AM tools of NDT. Between several other variables, the price, process effectiveness, form precision, heat ability, particular rigidity, longevity, and highest service heat of good blend machining can be identified by NDT [21]. Some of which are challenging properties to accomplish with polymer-based tools. But instead of using plastics, alloys are used in the machinery to accomplish greater usage conditions, higher levels of rigidity, and longer-lasting, more resilient machinery. Due to the excessive characteristic recovery and minimal surface hardness of laser powder bed fusion (L-PBF) procedures, it is now possible to create thin resources that are not just robust enough for extended production periods but also offer extra functionalities like incorporated cooling pathways and detectors. The creation of AM treat instruments is challenging to realise because there are currently few layouts for production processes that are efficient, just one repetition layout of intricately produced machinery optimised for energy consumption, even though the application of L-PBF techniques might be capable of accomplishing the desired machinery features NDT.

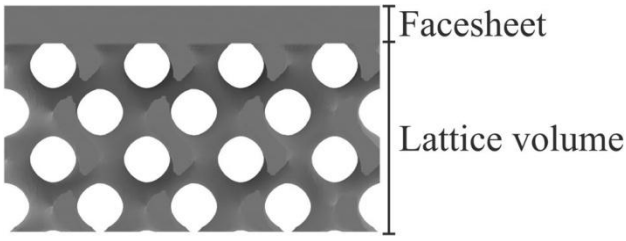

Figure 1: Suggested tooling side profile example

This work investigates the development and production of a novel AM mixture mould curing tool that incorporates mesh characteristics. The study is divided into subsequent parts. The framework and design recommendations for the device's production are described first. The laboratory approach, which includes AM construction characteristics, mixed healing techniques, and modelling approaches for evaluating the physical characteristics of the instruments and lattices, comes next. Heat and pressured putting of the oven method of curing will be used to test the L-PBF instruments' as-built areas. Lastly, the rigidity, temperature characteristics, and geometric precision in relation to analogous monolithic device layouts are used to evaluate the tool efficiency of NDT. The UK has stated that it is imperative to build the capacity to electronically create and manufacture future blended goods [47], emphasising the significance of this on a global level of NDT. With a focus on one-cycle layout, the study's findings are intended to serve as the foundation for drastically reducing the construction duration and the environmental effects of complicated tooling.

2. Tool design

2.1 Design specification

Since the goal of this research is to evaluate various tool geometry factors in order to obtain insight into AM tool design, the chosen mixed geometry wasn't a key feature. For maximum heat reactivity and dimensional precision, the optimal device would have an endlessly fragile, stiff, smooth, and completely flat facesheet. In the finished machinery, the layout's goal is to optimise all of these attributes. In order to maximise the examination ability, a modest, straightforward geometry was chosen to produce an abundance of devices for every AM build plate. A 100 mm by 100 mm area with a rigid face sheet and a mesh to stabilise the instrument was the selected device geometryNDT. The devices were made of stainless steel (316L). The face sheet area width at its smallest was roughly 0.7 mm, which is close to the production constraints and satisfies the

Licensed Under Creative Commons Attribution CC BY

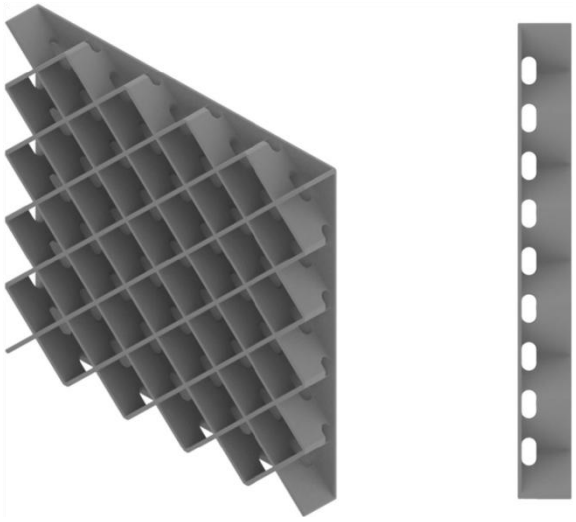

Figure 3: Alterations made to the conventional planar diamond lattice framework to encourage airflow via the matrix volume.

The dimension of a flat plate's area moment of flexing requires (Fig. 1).

Arrangements with recurring geometries that an individual cell may establish are called meshes. The minimally recurring single, or geometry, that is integrated to produce the broader framework of a mesh is called a single cellof NDT. Because they can enhance digestion of energy, heat transmission, and architectural benefits, they're a valuable tool in architecture. One benefit of additive manufacturing (AM) is its capacity to produce intricate geometries, such as mesh frameworks, that are impossible to produce using traditional additive methods of NDT. It will be feasible to develop and produce more lattice frameworks with even fewer individual cell dimensions and fewer volume proportion proportions (i.e., lower densities) as AM element quality and dependability continue to improve. To strengthen the thin facesheet, four mesh cell unit designs were chosen: a random mesh, a planar gemstone, a dual wall gyroid, and a gyroid (Fig. 2).

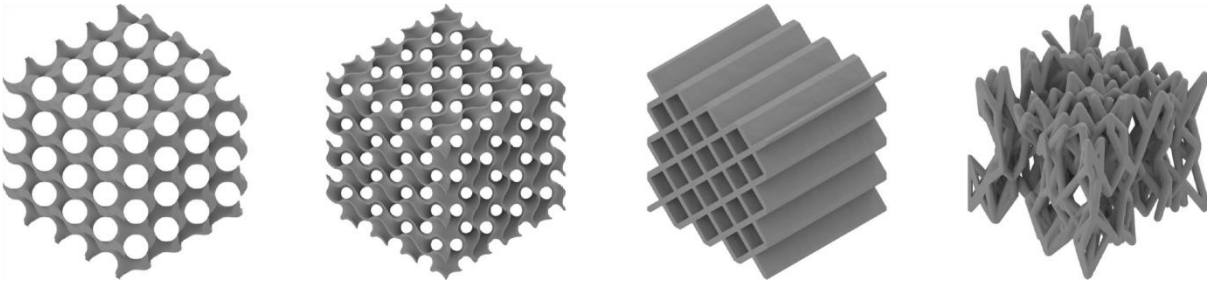

Figure 2: Random unit tissues, planar diamond, dual-wall gyroid, and repetition gyroid meshes (left-right order)

Table 1: Overview of instruments and unit cells for mesh geometry

Unit Cell	Lattice Density (%)	Lattice Geometry	Facesheet Thickness (mm)	ID
	15 (x2) 15 (x3)	Gyroid Gyroid	0.75 0.75	G.15(25-5).075.2 G.15(25-5).075.2
	46 (Thick strut) 46 (Thick strut) 24 (Thick strut) 24 (Thick strut) 20 (Thick strut) 20 (Thick strut)	Stochastic Stochastic Stochastic Stochastic Stochastic Stochastic	1 2 1 2 1 2	STk.46.1 STk.46.2 STk.46.3 STk.46.4 STk.46.5 STk.46.6
	15 (x5) 15 (x5)	Planar Diamond Planar Diamond	0.75 0.75	D.15(vd2).075.5 D.15(vd2).075.5
	46 46 26 26	Gyroid Gyroid Gyroid Gyroid	1 2 1 2	G.26.1 G.26.2 G.26.3 G.26.4
	10 (x10) 15 (x10) 10 (x8) 15 (x8) 5 (x5) 10 (x5) 10 (x5)	Planar Diamond Planar Diamond Planar Diamond Planar Diamond Planar Diamond Planar Diamond Planar Diamond	0.75 0.75 0.75 0.75 0.75 0.75 0.75	D.10.075.10 D.10.075.10 D.10.075.8 D.10.075.8 D.5.075.5 D.10.075.5 D.15.075.5
	20 40 40	Planar Diamond Planar Diamond Planar Diamond	2 1 2	D.26.2 D.40.1 D.40.2

A family of triply periodic minimum surface (TPMS) geometries that are characterised as meshes without connections or imperfections are gyroid and dual wall gyroid single cells. Large particular elasticity and substantial surface spaces in relation to the total volume are characteristic features of these designs.The gyroid and other TPMS lattices are often used when lightweight parts are needed because of these qualities of NDT [48, 49]. They are

Licensed Under Creative Commons Attribution CC BY

used for mechanical and acoustical filtering purposes [52, 53], AM warmth exchangers, and warmth sinks [50, 51]. Given the particular rigidity inherent in both types of gyroid mesh, mixture lamination and fix technologies could be useful in this instance enhance the device's fundamental characteristics and provide more surface space for better laminar heat transmission of NDT. Random lattices, on the other hand, are frameworks that are arbitrarily produced and are possible to accomplish using techniques like coronoid tessellation [54] or other methods involving pseudo-randomness. Such lattices, which have asymmetric unit geometries, enable arbitrary point creation or adjustable arches to specify the comprehensive geometry [56]. Employing a random mesh provides advantages including strong particular rigidity, effect, and shear resistance thermal stability, appropriate damping qualities, and satisfactory biocompatibility [57]. The general rigidity of stitches It has been discovered that tic meshes are greater than that of comparable meshes because of their volume energy isotropic mesh [54], which is especially useful in surgical implants [58, 59] and further mechanical parts with a very particular rigidity requirement. Nevertheless, producing random meshes with particular problems can make achieving the necessary mechanical qualities challenging. Concerning the capacity to manufacture and the huge amount of data character characteristic of asymmetric geometries as STL files The purpose of employing In this case, a random mesh is used to preserve the stiffness of the instrument while utilising the unpredictability of the construction by adding more turbulence to the airflow under the device's appearance, boosting its possible heat transmission via the component [60].

The horizontal crystal mesh, a straightforward geometry that provides the necessary rigidity, was the last matrix geometry to be studied of NDT. However, there are drawbacks to employing a planar mesh in an autoclave, such as reduced ventilation via the instrument's bottom. Including holes in the walls to encourage wind within the oven's flow for more uniform warming throughout every layer is one way to mitigate this (Fig. 3). It was chosen over a honeycomb-style topology because the 45° angle of the gem topology lets L-PBF make it without having to use support structures or basic cell size limits to keep the surfaces smooth throughout the construction quantity of NDT. In order to maximise the lattice mechanical characteristics, the planar checkerboard's intrinsic compactness allows for the inclusion of scaled porosity meshes [61], geographically uneven planar meshes [62], or hierarchical planar meshes [63]. The technology for indirect training, Gen3D, was used to develop all of these characteristics [64, 65].The four web geometries are the basis for the differences in flat-surface device geometries of NDT. The mesh weight, cell unit dimension, strut width, face sheet width, and mesh type that were previously mentioned were all altered in every device test of NDT. Particular modifications to the gyroid and flat stone topologies were given in addition to the four network topologies. With a 5% volume at the bottom and a 25% intensity at the device exterior, two variants of scaled gyroid networks were examined. This added weight increased the rigidity and encouraged thermal conduction in the area near the device area and diffusion over the entire curing cycle of NDT. At the ends of two versions of the PLA-nar gem network, there were 2 to 3 mm holes. the diamonds to encourage air movement amongst the individual cells. The last requirements for device net design are compiled in Table 1, and the device name sources' terminology is detailed as follows:

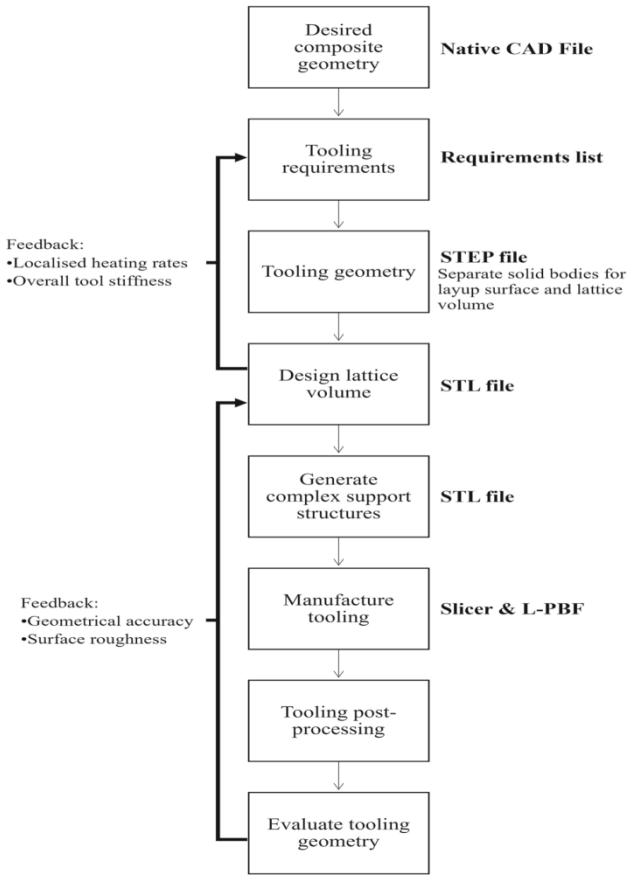

Figure 4: A suggested DfAM architecture for creating customised AM blend tools

Table 2: Construction characteristics of the Renishaw AM250

Unit	Value	Parameter
µm	50	Layer Height
µs	80	Exposure Time
µm	110	Hatch Spacing
W	200	Laser Power
µm	60	Point Distance
µm	10–40	Powder Size

2.2 Design framework

The structure for the Creation for AM (DfAM) process is shown in Figure 4, which enables the creation of customised AM mixture tools. The study aims to offer insight into the behaviour of various topologies in this programme, which will aid in designing the network sizes and facesheets.

3. Experimental Method

3.1 Tool manufacturing

316L aluminium alloy (SS316L) powder was used to make metal instruments on Renishaw AM250 L-PBF equipment. Because of its similarities with instrument iron and its simplicity of manufacturing using L-PBF AM, SS316L was chosen of NDT. Table 2 summarises other construction

Licensed Under Creative Commons Attribution CC BY

procedure factors. For every tool, two complete construction discs were needed, and the assembly plate and procedure settings remained the same in both constructions. To improve powder distribution, lessen harm to the wiper blade, and accommodate a maximum of 16 devices on every construction dish, the instruments were positioned on their sides with the facesheet pointing slightly away from the y-z axis (Fig. 5). Light-grain sandpaper was employed to get any completely fused powder fragments off the facesheet prior to building up the mixture of pre-peg coatings, and the instruments were properly cleaned to make sure that no powder remained on the component. After eliminating the foundation frameworks from the bottom, the tools were not further post-processed. Maintaining an almost as-built condition on the AM devices allows for an early evaluation of AM machining and reduces the time and money required to create every instrument NDT. To guarantee flatness, the device's geometrical precision was assessed. After being taken out of the manufacturing dish, each instrument's top layer was imaged with a CMS108Ap laser detector and a 7-axis Romer Perfect Arm 7535 SE by Hexagon Meteorology. The resultant point's additional processing

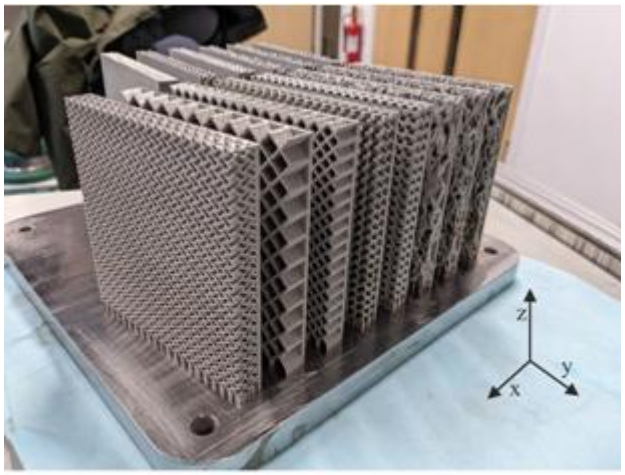

(a) AM Build 1 (14 Tools)

(b) AM Build 2 (16 Tools)

Figure 5: AM Assembly of every 30 instruments: AM Develop 1 (a) with 14 tools; AM Develop 2 (b) with 16 tools

Cloud computing was done using MATLAB [66]. A mean area was computed following the application of a matrix of transformations to align every point cloud information spot with the X-Y plane. The exterior deviation was determined by taking the top 5% of maximum values, which were derived from the separation scale of every point in the focal cloud from the mean appear, to get the stated smoothness scores.

3.2 Composite fabrication and substance

Pre-impregnated (pre-preg) fabric (MTC400-C415T-T700-12K-38%RW-1250) was utilised. It consisted of a twill weave cloth reinforced with T700 carbon fibre within a hardened substrate of SHD MTC400 epoxy glue.

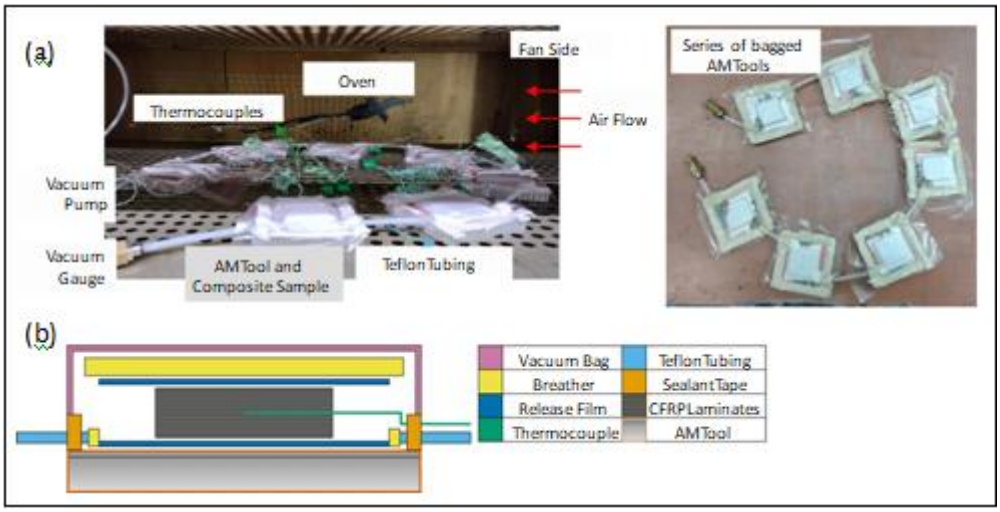

Figure 6: Diagram showing the daisy-chain linkage of AM machines in the packing scheme.

Fourteen layers of 40 mm x 40 mm pre-preg were used to make the mixture laminate so that the theoretically healed part would be 7 mm thick. Among the 7th and 8th layers of the F system, a thermostat was inserted to record the temperature throughout the curing procedure NDT. The mixture was prepared on the AM equipment using the conventional blend hoover packing strategy (Fig. 6). Using PTFE containers, numerous instruments were daisy-chained

Licensed Under Creative Commons Attribution CC BY

together to decrease the overall number of healing sessions while maintaining the limitations of just one vacuum engine OF NDT. To make certain the pouch could withstand a vacuum force of as high as 100 kPa, its condition was examined.

After that, the ready-made instruments were put in a regular oven (carbolite) to cure. Temperature information was gathered at a sampling speed of 1 Hz using thermostats that were attached to a Pico Logger datalogger. The vendor's quickest cure timetable was subsequently followed in order to heal the combined piecesNDT. The therapy plan was 3 °C/ min to 135 °C, with a 1-hour stay for complete cure and a 2-°C/ min cool-down to 30 °C after that.

3.3 Physical data processing

The exceeded temperature and the device's warming speed in relation to the oven, as described in Section 3.2, were used to assess the devices' heat sensitivityNDT. The temperature sensor information was used to determine the temperature rise and overrun for the various instrument geometries (Fig. 7). Before, the warmth rate was found in the first 1000–2000 s of each instrument's temperature profile. This is because this area depends only on the instrument and furnace and happens after the temperature reaches equilibrium. Since the trend is going up, it looks like the polymer isn't changing chemically. Instead, heat exchange, not the exothermic method, is the main process OF NDT. The variation between the oven's maximum heat and its programmed heat was used to compute the warmth overrun. Since polyurethane cures by an exothermic response, excessive power creation throughout the procedure may result in heat rising over the oven's interior if the rate of warmth is high and the levels of heat transfer via the oven are sufficiently low. This heat overrun can

Fig. 7 Sample temperature history of one tool during the oven curing process

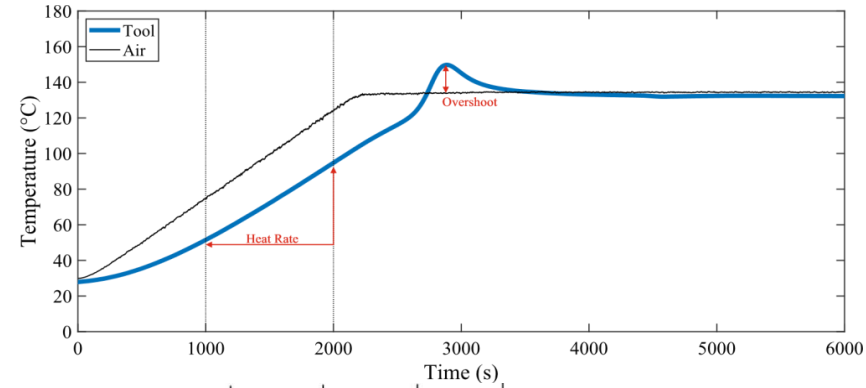

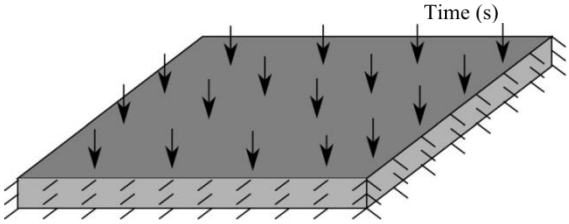

Figure 8: The four sides of each plate were clamped together, and a constant pressure (P) of 0.1 MPa was applied to the solid (non-lattice) face on top of each plate

Describe the instrument's temperature reaction in terms of how well it controls the temperature overrun and how well heat is transferred into the mixed product OF **NDT**. To ascertain which instrument had the highest potential for more intricate compound geometries, all of these measurements were contrasted with one another and with the predicted instrument tension.

3.4 Modelling tool stiffness

Employing the Simpleware Scan IP programme, 3-D volume models were produced from the STL data [67]. The dimension of the voxels was defined using the resampling operation, and it was set to 0.5 mm cubes. Before integrating the component into the programme, the STL was initially transformed into a voxel filter. This allowed the programme to connect the component independently of the already-present STL ground texture and could be deployed uniformly to all meshes. The programme produced tetrahedral grids with a variety of strengths of NDT. The supplemental material contains a summary of the resulting texture quality indicators.

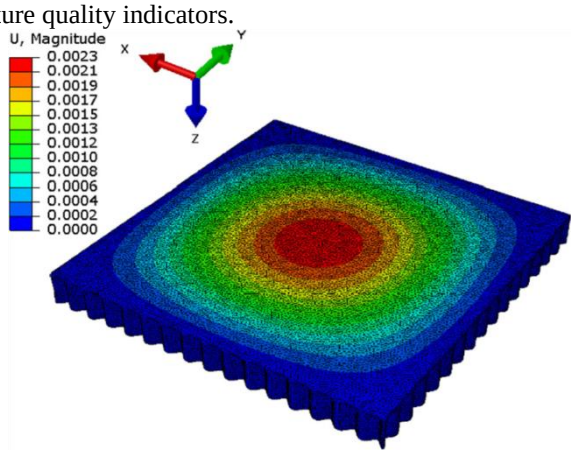

Figure 9: Shows a typical curve map of the simulation outcomes with a 40% volume percentage diamond mesh. Size of dislocation in millimetres

Licensed Under Creative Commons Attribution CC BY

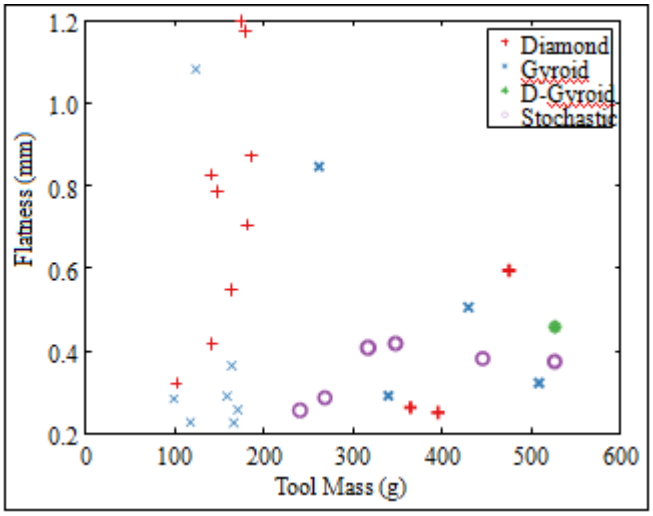

Figure 10: Calculated device tension in relation to the smoothness of the produced device

Finite component construction with the implied dynamic solver in the application ABAQUS was used to quantify the instrument's rigidity [68]. Steel's elastic linear characteristics (E = 200 GPa, v = 0.3) were determined using quadratic tetrahedral components (C3D10). The four lateral corners were secured in all directions while a force load of 0.1 MPa was applied to the top device surface (Fig. 8). The device's lateral movement amplitude was computed, and Fig. 9 displays a contour map of a representative design of NDT. The dual-walled gyroid matrix design (Fig. A1) was used to conduct a network resolution investigation, and the results showed that the greatest displacement values resolved at 1.22 million components with an average component border length of 0.83 mm. Additionally, the results of sheet displacement were contrasted with

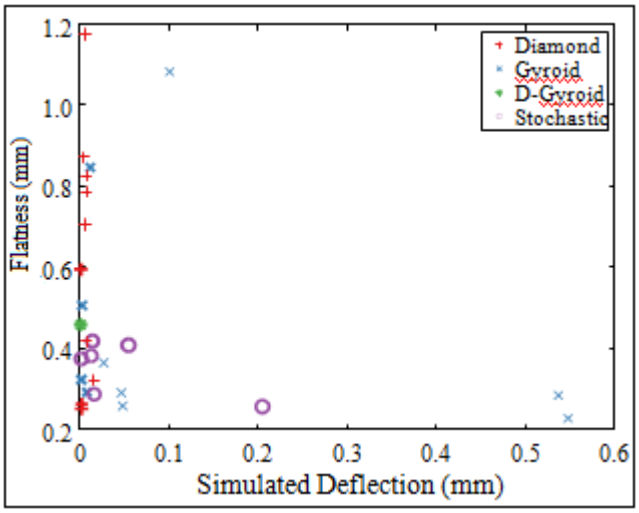

Table 11: Device surface smoothness derived from total machine mass

those of solid square sheets with (a) similar thickness and (b) similar quantity, and the comparative deformation values discovered for every mesh were as follows:

Relative deflection = $\frac{Lattice\ \ deflection}{Equivalent\ \ solid\ deflection}$

4. Results

4.1 Geometrical accuracy

The fact that about 80% of the instruments have a small bending structure shows that some thermal expansion happened during the generation process because the AM construction room was too hot. Even with no afterwards The bulk of the instruments showed distortion of less than one millimetre after heat therapy to remove this remaining tension. The only instruments with total errors larger than 1 mm were D.15.075.8, D.15(vd2).075.5, and G.10.075.2. The predicted device tension (Fig. 10) and the geometric precision of the instruments did not significantly correlate, despite the possibility that the decreased tension in comparison to a strong monolithic device could cause heat distortion. On the other hand, Fig. 11 illustrates the connection between the instrument's weight and facesheet smoothness of NDT. It is evident that the more lightweight devices result in poorer levels of flatness, even though the connection wasn't precisely proportionate of NDT. This suggests there's less core weight and less network stability. But it is conceivable to have thin, flat instruments. Supplementary Section B contains more correlations between the instrument's smoothness and the remaining three design factors.

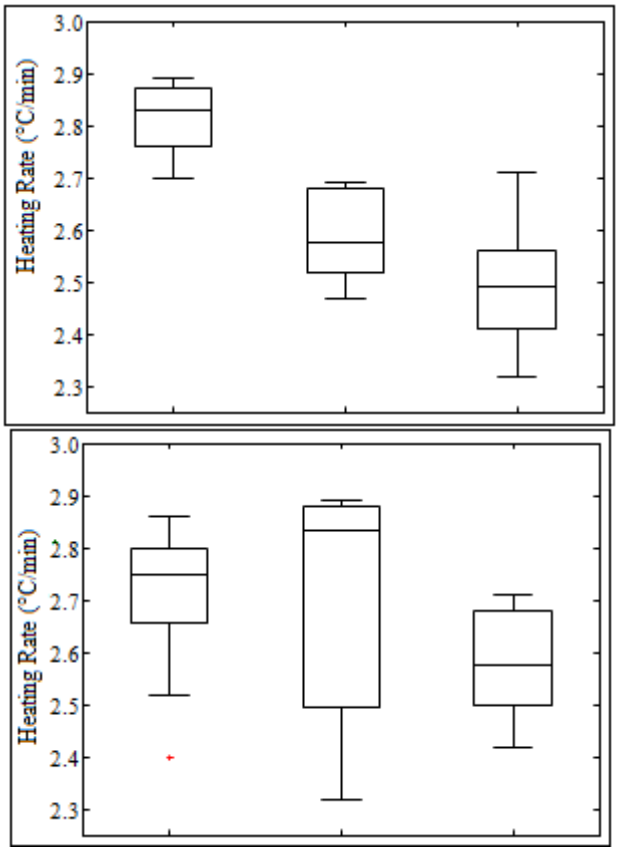

Licensed Under Creative Commons Attribution CC BY

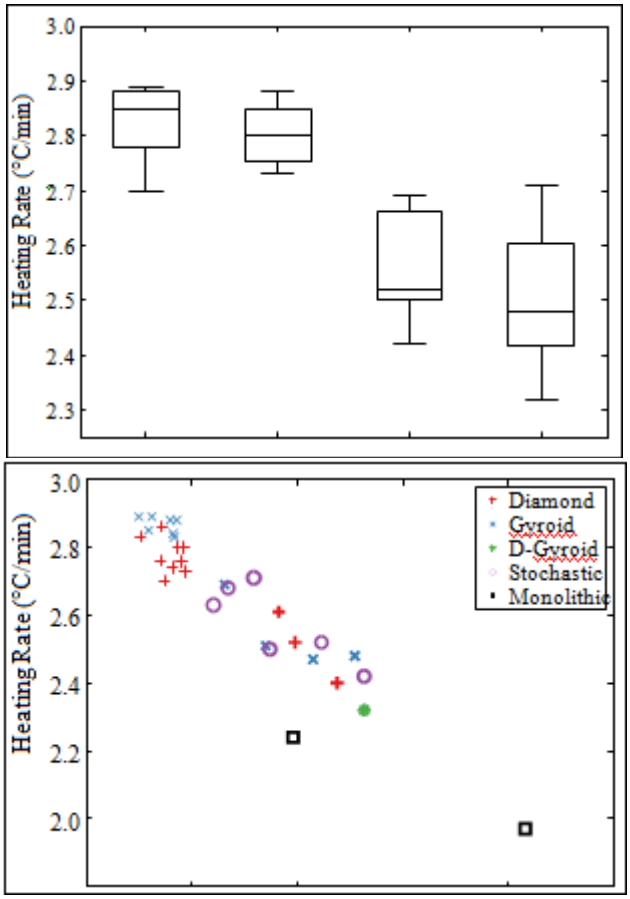

Figure 12: Warming frequency of all 30 instruments throughout the cure phase: There are four different ways to calculate the composite warming rate: (a) facesheet thickness; (b) web topologies; (c) network densities; and (d) total instrument weight.

4.2 Thermal responsiveness

An overview of the thermocouple findings by means of the observed temperature rise and overrun degrees is displayed in Figures 12 and 13. According to preliminary patterns, the weight of the instruments was directly correlated with the overrun warmth (Fig. 13d) and the warmth rate (Fig. 12d). However, because the 0.75 mm thick sheet with gyroid networks varied from the straight pattern, the excess heat rise wasn't equal. This reaction was particularly displayed by the instruments that had the graded mesh in the z axis. It was advantageous to have higher void fractions at the bottom of the instrument's mesh dimension in conjunction with a raised instrument weight close to the faceplate. Further velocity across the mesh container and the increased stuff close to the bottom were caused by a reduced mesh concentration at the bottom. The faceplate's function as a thermal drain assisted in lowering the exotherm's amplitude of NDT. The instruments studied in this study were capable of accomplishing quicker heating speeds due to their comparable instrument weight when contrasted with 5 mm and 10 mm-thick massive implements (Fig. 12d). Because of the reduced warming rates, the huge devices were able to decrease the size of the overrun (Fig. 13d). As illustrated by Fig. 14, this pattern held true for all 30 devices as well as the two massive devices. It's evident that the surface width significantly affected the device's temperature rise (Fig. 12a) and temperature overrun (Fig. 13a). Because there were fewer components for the atmosphere to warm up before it might heal the combined epoxy, the thinner sheets permitted a quicker pace of warming of NDT. A significant distinction ($p < 0.001$) was observed when evaluating the 0.75 mm discs with the 1.00 mm and

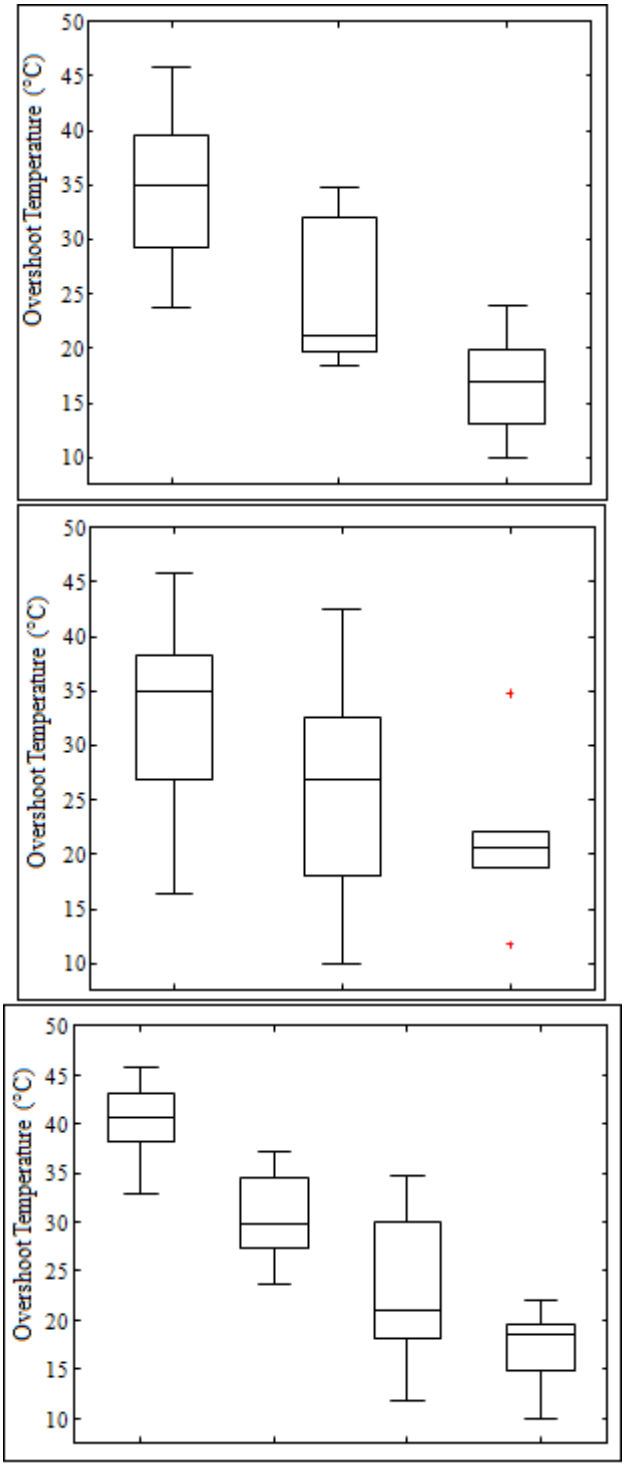

(c) The mesh density-related heat overrun.

Licensed Under Creative Commons Attribution CC BY

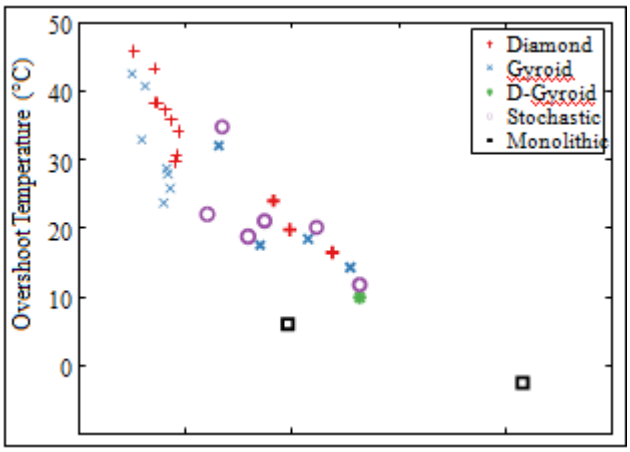

(d) Overshoot in temperature due to total device weight

Fig. 13 Thermal overshoot during curing of all thirty tools: (a) Thermal overshoot based on facesheet thickness; (b) Thermal overshoot based on lattice geometries; (c) Thermal overshoot based on lattice density; (d) Thermal overshoot based on overall tool mass.

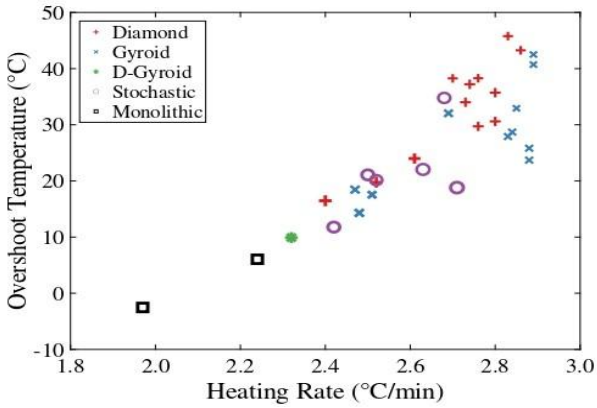

Figure 14: Thermal overshoot and heating rate: a relationship.

The overshoot can be attributed to various factors, including facesheet width, network geometry, network density, and total device weight layers measuring 2.00 mm, but not in between these two heavier layers. However, the higher mesh frequencies utilised in these instrument examples may have lessened the influence of the particular panel width, thus decreasing the influence of the distinction between the 1.00 mm and 2.00 mm panels. Likewise, there was a substantial difference in the impact of the plate width on temperature overrun between 0.75 mm and 1.00 mm ($p < 0.01$) and 2.00 mm ($p < 0.001$), but not among the two wider panels. The overrun effect was lessened by the instruments with slower heating speeds and, thus, more thermal weight, which resulted in reduced overrun heat on the heavier and more dense instruments. Regarding the whole lattice framework geometry chosen, there was no particular reliance on the device temperature rise (Fig. 12b) or overrun (Fig. 13b). The associations between the network's frequency and the warming speed and temperature overrun, respectively, are depicted in Figures 12c and 13c. Given that the network thickness was directly related to the total device weight, the outcomes were consistent with the previously mentioned connections. When contrasting the set lower than 20% with the group higher than 20%, the warmth rate demonstrated a substantial reliance on the mesh's thickness ($p < 0.001$). There was an important distinction ($p < 0.01$) between the thinnest density range (≤ 10%) and the spectrum from 11 to 20%, as indicated by the temperature overrun. This suggests that, although the temperature rise was more dependent on facesheet width, the excess heat seems to be proportionate to mesh weight, irrespective of facesheet depth.

4.3 Tool stiffness

The facesheet devices anchored to random networks exhibited the least rigidityNDT, as seen in Figure 15. One mesh displayed a deformation that was more than 650 times that of a solid surface with a comparable width (depending on the depth of the gadget facesheet). Every single one of the

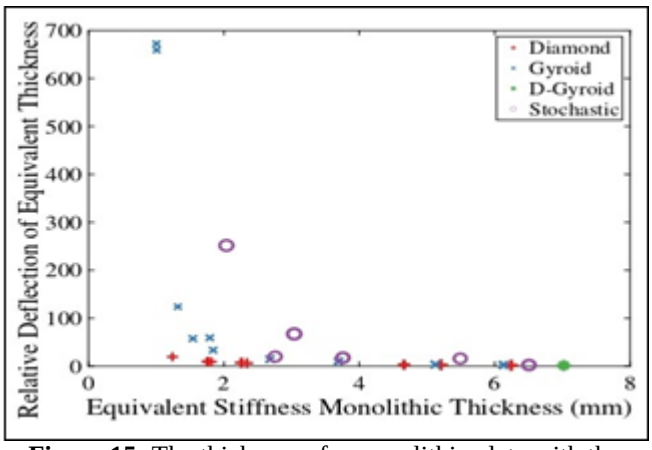

Figure 15: The thickness of a monolithic plate with the same stiffness plotted against the relative deflection of a solid plate with the same thickness.

The refraction scales of networks were larger than those of a solid plate of the same width. As the weight is eliminated, the actual stretching rigidity would decrease for a given amount and thickness. Because it possessed the largest weight of all devices created, the D-Gyroid has a firmness that is nearest to that of a hard sheetof NDT. The mesh detours were comparable to the solid surfaces (Fig. 16) when the comparative displacement to an equal capacity instrument (based on a solid object equal to the whole device capacity) was evaluated, highlighting the significance of mesh thickness to the device rigidity behaviour of NDT. But the lattice framework also played a role; some of the random networks had over two times the deformation of the same-sized hard dish, despite the fact that most lattice arrangements had lesser deflections.

Licensed Under Creative Commons Attribution CC BY

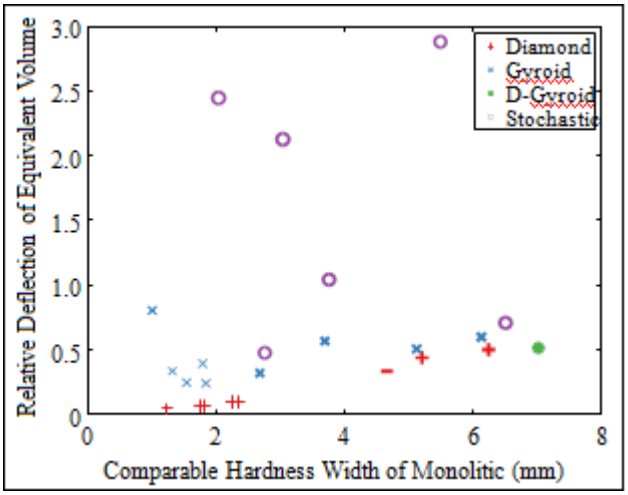

Figure 16 shows a scatter chart of the comparative deformation of a comparable quantity of thick sheet vs. the width of a similarly rigid massive panel redirected. The stone lattices, on the other hand, showed the least comparative distortion. The comparable capacity device's comparative flexion is significantly less than that of the corresponding depth instruments, suggesting that choices about porosity layout and network geometry have a significant influence on the device's total rigidity.

5. Discussion

The next was discovered as a consequence of evaluating these factors for the mixture healing on an original geometry with little post-processing: First of all, the repair devices all retained their suction purity while withstanding the pressure of the suction and heat stress. Since every tool had a restricted amount of afterwards therapy (to help enhance the facesheet's top quality), it was crucial to make certain the as-constructed top could withstand a hoover using traditional sacking methods. Second, the meshes demonstrated potential as a weight reduction technique and a way to control the temperature characteristics. Regarding the weight decrease, calculations of NDT revealed that the massive equal was stronger than each AM instrument counterpart, even though every example had enough rigidity to be employed in a single instance while keeping a uniform device capacity. Therefore, throughout the layout phase, consideration should be given to the network shape, weight, and total tool rigidity. Each AM device's thermal characteristics were enhanced in comparison to a massive device of the same size because the tools' airflow prevented overrun and allowed for an appropriate chilling percentage, and their average temperature rises were higher of NDT. Furthermore, an intriguing chance to further benefit from using AM to create and manufacture the mixture mould equipment is presented by the option to choose a certain network morphology for an ideal thermal efficiency over a wider device geometry with increasing intricacy.

By maximising the device warming speed in relation to its geometric precision as the two deciding parameters, the mesh topologies and corresponding layer thickness that show the greatest potential were evaluated. The connection between these two factors is depicted in Figure 17, with tools with high rates of heating and a greater level of geometrical precision shown by the ideal reaction in the bottom right quadrant. It demonstrates that, generally, the low-mass devices performed better because of their thin facesheet and reduced mesh weight, which resulted in a temperature rise of about 3 C/min. The best tool efficiency was achieved by the gyroid lattice-based instruments, which showed substantial temperatures while maintaining modest area variations. In particular, the scaled gyroid networks performed most highly in terms of heat responsiveness, particular rigidity, and geometrical correctness (Fig. 17). Although the current research's findings demonstrate small-scale benefits over massive devices,

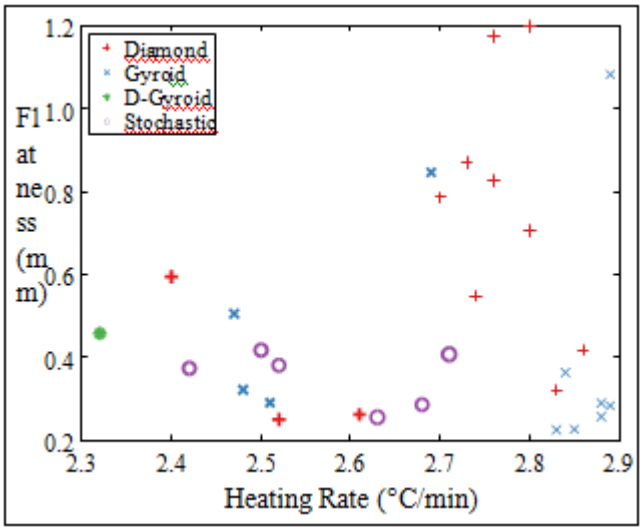

Figure 17: Modification of top tools Line width and marker length are correlated with facesheet depth and network weight, respectively.

To raise the degree of technological preparedness, more research into using these creation methodologies for bigger and more intricately shaped combined devices is required. Given that the instruments were evaluated in their as-constructed condition, certain scenarios may find the facesheet surface texture to be inadequate. However, post-processing techniques like cutting the facesheet where the mixture will come into direct contact with it throughout the cooling phase may solve this. Likewise, post-machining of the facesheet to enhance the surface texture will become less necessary as the upcoming AM and L-PBF methods increase in grade. Research on optimising roughness of surfaces via laser inspection and construction tactics has demonstrated that R a ≈ 9μm can be achieved for alloys of copper [69], R a ≈ 4μm and below for AlSi10Mg [70], and SS316L can reduce exterior texture by greater than R a = 10μm to R a ≈ 20μm [70]. Future research will concentrate on techniques for increasing the final component dimension, additional processing of the instrument and facesheet areas, and examination of the unique characteristics and optimisation of the framework frameworks.

6. Conclusion

This study highlights the possibility of creating new kinds of polymer tools through additive manufacturing. Improved temperature quickness, the capacity to manage the healing exotherm more controllably, and greater designin NDT

Licensed Under Creative Commons Attribution CC BY

freedom to allow device geometry optimisation to produce the required tool characteristics and precision were the three benefits realised. In an oven repair period, the scaled gyroid lattice-based devices' thermal efficiency was capable of reaching above 93% of the utilised warming rate in NDT. These thin devices possessed rigidity equal to that of a massive instrument, over 2.5 times the facesheet width. Mesh constructions with higher densities attained a 2 mm AM machine had the same machine rigidity of a massive tool up to 3.5× the facesheet depth (the rigidity of a monolithic 7 mm tool). Employing mesh geometries, the instruments produced a maximum rise in warming velocity as opposed to their massive counterparts of the same weight of NDT. Considering geometrical factors' impacts on the instruments, the findings demonstrated that the temperature overshoot Fig. 13c shows a stronger correlation with network thickness. yet the facesheet had a greater influence on the warming speed. proportions (Fig. 12a). 30 devices were tested, and the rated the two most promising sheets were gyroid mesh-based ones. lattice configurations because they enhanced airflow beneath the facesheet in order to preserve the appropriate energy density and rigidity when needed. Utilising AM creates a novel chance for a change in perspective in the mixture machining business. The findings of this study indicate an innovative method for creating a brand-new kind of mould instrument. It could have big effects on the materials sector.

References

[1] Li C, Pisignano D, Zhao Y et al (2020) Advances in medical applications of additive manufacturing. Engineering 6(11):1222–1231.https://doi.org/10.1016/j.eng.2020.02.018

[2] Salmi M (2021) Additive manufacturing processes in medical applications. Materials 14(1):1–16. https://doi.org/10.3390/ma14010191

[3] Patel P, Gohil P (2021) Role of additive manufacturing in medical application COVID-19 scenario: India case study. J Manuf Syst 60(November 2020):811–822. https://doi.org/10.1016/j.jmsy.2020.11.006

[4] Deisenroth DC, Moradi R, Shooshtari AH et al (2018) Review of heat exchangers enabled by polymer and polymer composite additive manufacturing. Heat Trans Eng 39(19):1652–1668. https://doi.org/10.1080/01457632.2017.1384280

[5] Scheithauer U, Schwarzer E, Moritz T et al (2018) Additive manufacturing of ceramic heat exchanger: opportunities and limits of the lithography-based ceramic manufacturing (LCM). J Mater Eng Perform 27(1):14–20. https://doi.org/10.1007/s11665-017-2843-z

[6] Tiwari R, Andhare RS, Shooshtari A et al (2019) Development of an additive manufacturing-enabled compact manifold microchannel heat exchanger. Appl Ther Eng 147(April 2018):781–788. https://doi.org/10.1016/j.applthermaleng.2018.10.122

[7] Kaur I, Singh P (2021) State-of-the-art in heat exchanger additive manufacturing. Int J Heat Mass Trans 178(121):600. https://doi. org/10.1016/j.ijheatmasstransfer.2021.121600

[8] Diegel O, Schutte J, Ferreira A, et al (2020) Design for additive manufacturing process for a lightweight hydraulic manifold. Additive Manufacturing 36(June):101,446. https://doi.org/10.1016/j.addma.2020.101446

[9] Blakey-Milner B, Gradl P, Snedden G et al (2021) Metal additive manufacturing in aerospace: a review. Mater Des 209(110):008. https://doi.org/10.1016/j.matdes.2021.110008

[10] Khorasani M, Ghasemi AH, Rolfe B et al (2022) Additive manufacturing a powerful tool for the aerospace industry. Rapid Prototyping Journal 28(1):87–100. https://doi.org/10.1108/RPJ-01-2021-0009

[11] Yang S, Min W, Ghibaudo J et al (2019) Understanding the sustainability potential of part consolidation design supported by additive manufacturing. J Cleaner Production 232:722–738. https://doi.org/

[12] 10.1016/j.jclepro.2019.05.380 12. Huang R, Riddle M, Graziano D et al (2016) Energy and emissions saving potential of additive manufacturing: the case of lightweight aircraft components. Journal of Cleaner Production 135:1559–1570. https://doi.org/10.1016/J.JCLEPRO.2015.04.109

[13] Hanaphy P (2022) SLM solutions to develop “world’s largest” metal 3D printer for the us air force. https://3dprintingindustry. com/news/slm-solutions-to-develop-worlds-largest-metal-3dprinter-for-the-us-air-force-215010/

[14] Enable Manufacturing Ltd. (2021) New Vacuum Additive Casting process set to rock the metal 3D printing world. https://enable. parts/2021/05/new-vacuum-additive-casting-process-set-torock-the-metal-3d-printing-world

[15] British Standards Institution (2022) BS EN ISO/ASTM 52900:2021 - Additive manufacturing - General principles - Fundamentals and vocabulary. Tech. rep, British Standard Institution

[16] Papadakis L, Avraam S, Photiou D, et al (2020) Use of a holistic design and manufacturing approach to implement optimized additively manufactured mould inserts for the production of injection-moulded thermoplastics. J Manuf Mater Process 4(4). https://doi.org/10.3390/jmmp4040100

[17] Hassen AA, Lindahl J, Springfield R, et al (2016) The durability of large-scale additive manufacturing composite molds. In: CAMX Conference Proceedings, Anaheim, CA, https://www.researchgate. net/publication/324391116

[18] Sudbury TZ, Springfield R, Kunc V et al (2017) An assessment of additive manufactured molds for hand-laid fiber reinforced composites. Int J Adv Manuf Technol 90(5–8):1659–1664. https://doi.org/10.1007/s00170-016-9464-9

[19] Hassen AA, Noakes M, Nandwana P, et al (2020) Scaling Up metal additive manufacturing process to fabricate molds for composite manufacturing. Additive Manufacturing 32(March 2019):101,093. https://doi.org/10.1016/j.addma.2020.101093

[20] Sharma A, Johnson B (2020) UK sets ambitious new climate target ahead of UN Summit. Tech. rep., https://www.gov.uk/ government/news/uk-sets-ambitious-new-climate-target-aheadof-un-summit

Licensed Under Creative Commons Attribution CC BY

[21] Li Y, Xiao Y, Yu L, et al (2022) A review on the tooling technologies for composites manufacturing of aerospace structures: materials,structures and processes. Composites Part A: Applied Science and Manufacturing 154(June 2021):106,762. https://doi.org/10.1016/ j.compositesa.2021.106762
[22] Centea T, Peters G, Hendrie K et al (2017) Effects of thermal gradients on defect formation during the consolidation of partially impregnated prepregs. Journal of Composite Materials 51(28):3987–4003. https://doi.org/10.1177/0021998317733317
[23] Mirzaei S, Krishnan K, Al Kobtawy C et al (2021) Heat transfer simulation and improvement of autoclave loading in composites manufacturing. Int J Adv Manuf Technol 112(11–12):2989–3000. https://doi.org/10.1007/s00170-020-06573-3
[24] Song YS, Youn JR, Gutowski TG (2009) Life cycle energy analysis of fiber-reinforced composites. Composites Part A: Applied Science and Manufacturing 40(8):1257–1265. https://doi. org/10.1016/j.compositesa.2009.05.020.www.sciencedi rect.com/ science/article/pii/S1359835X09001687
[25] Duflou JR, De Moor J, Verpoest I et al (2009) Environmental impact analysis of composite use in car manufacturing. CIRP Annals 58(1):9–12. https://doi.org/10.1016/j.cirp.2009.03.077. www.sciencedirect.com/science/article/pii/S0007850609000304
[26] Lai X, Wang C, Peng D et al (2021) Analysis of heat transfer characteristics of a heat exchanger based on a lattice filling. Coatings 11(9):1–13. https://doi.org/10.3390/coatings11091089
[27] Koneri R, Mulye S, Ananthakrishna K et al (2021) Additive manufacturing of lattice structures for heat transfer enhancement in pipe flow. Springer Singapore. https://doi.org/10.1007/978-981- 15-5689-0_21
[28] Tian Y, Zhao CY (2011) A numerical investigation of heat transfer in phase change materials (PCMs) embedded in porous metals. Energy 36(9):5539–5546. https://doi.org/10.1016/j.energy.2011. 07.019
[29] Rehman Tu, Ali HM, Janjua MM et al (2019) A critical review on heat transfer augmentation of phase change materials embedded with porous materials/foams. Int J Heat Mass Trans 135:649–673. https://doi.org/10.1016/j.ijheatmasstransfer.2019.02.001
[30] Sajjad U, Rehman Tu, Ali M et al (2022) Manufacturing and potential applications of lattice structures in thermal systems: a comprehensive review of recent advances. Int J Heat Mass Trans 198(123):352. https://doi.org/10.1016/j.ijheatmasstransfer.2022.123352
[31] King D, Tansey T (2003) Rapid tooling: selective laser sintering injection tooling. J Mater Process Technol 132(1–3):42–48. https:// doi.org/10.1016/S0924-0136(02)00257-1
[32] Kovács JG, Szabó F, Kovács NK et al (2015) Thermal simulations and measurements for rapid tool inserts in injection molding applications. Appl Ther Eng 85:44–51. https://doi.org/10.1016/j.applthermaleng.2015.03.075
[33] Bard J, Cupkova D, Washburn N et al (2018) Robotic concrete surface finishing: a moldless approach to creating thermally tuned surface geometry for architectural building components using Profile-3D-Printing. Construction Robotics 2(1–4):53–65. https://doi.org/10.1007/s41693-018-0014-x 34. Zink B, Kovács NK, Kovács JG (2019) Thermal analysis based
[34] method development for novel rapid tooling applications. Int Commun Heat Mass Trans 108(August):104,297. https://doi.org/10.1016/j.icheatmasstransfer.2019.104297
[35] Bagalkot A, Pons D, Clucas D et al (2019) A methodology for setting the injection moulding process parameters for polymer rapid tooling inserts. Rapid Prototyping Journal 25(9):1493–1505. https://doi.org/10.1108/RPJ-10-2017-0217
[36] Sama SR, Badamo T, Manogharan G (2020) Case studies on integrating 3D sand-printing technology into the production portfolio of a sand-casting foundry. Int J Metalcasting 14(1):12–24. https:// doi.org/10.1007/s40962-019-00340-1
[37] Yang Y, Li H, Xu Y et al (2019) Fabrication and evaluation of dental fillers using customized molds via 3D printing technology. Int J Pharma 562(December 2018):66–75. https://doi.org/10.1016/j.ijpharm.2019.03.024
[38] Seleznev M, Roy-Mayhew JD (2021) Bi-metal composite materialfor plastic injection molding tooling applications via fused filament fabrication process. AdditiveManufacturing 48(PA): 102,375. https://doi.org/10.1016/j.addma.2021.102375
[39] Kuo CC, Lin BH, Luo ZT (2022) A new hybrid process combiningrapid tooling and machining to manufacture an injection mold withmicro features. Int J Adv Manuf Technol 119(9–10):6349–6360.https://doi.org/10.1007/s00170-021-08529-7
[40] Masood SH, Song WQ (2004) Development of new metal/polymermaterials for rapid tooling using Fused deposition modelling.Materials and Design 25(7):587–594. https://doi.org/10.1016/j.matdes.2004.02.009
[41] Luši´c M, Schneider K, Hornfeck R (2016) A case study on thecapability of rapid tooling thermoplastic laminating moulds formanufacturing of CFRP components in autoclaves. Procedia CIRP50:390–395. https://doi.org/10.1016/j.procir.2016.04.151
[42] Rodríguez-Parada L, Mayuet PF, Gámez AJ (2019) Industrialproduct design: study of FDM technology for the manufactureof thermoformed prototypes. Proc Manuf 41:587–593. https://doi.org/10.1016/j.promfg.2019.09.046
[43] Bere P, Neamtu C, Udroiu R (2020) Novel method for the manufacture of complex cfrp parts using fdm-based molds. Polymers12(10):1–20. https://doi.org/10.3390/polym12102220
[44] Murdy P, Dolson J, Miller D et al (2021) Leveraging the advantagesof additive manufacturing to produce advanced hybrid composite structures for marine energy systems. Appl Sci (Switzerland)11(3):1–15. https://doi.org/10.3390/app11031336
[45] Hassen AA, Lindahl J, Chen X, et al (2016) Additive manufacturing of composite tooling using high temperature thermoplasticmaterials. In: SAMPE

Licensed Under Creative Commons Attribution CC BY

conference proceedings, Long Beach, CA,https://www.researchgate.net/publication/324442073

[46] Kunc V, Lindahl J, Dinwiddie R, et al (2016) Investigationof in-autoclave additive manufacturing composite tooling. In:CAMX conference proceedings, Anaheim, CA, http://energy.gov/downloads/doe-public-access-plan

[47] Grassi M, Smith F (2019) Aerospace composite technologyroadmapping. In: Composites Leadership Forum

[48] Zheng X, Lee H, Weisgraber TH et al (2014) Ultralight, ultrastiffmechanical metamaterials. Science 344(6190):1373–1377. https://doi.org/10.1126/science.1252291

[49] Schaedler TA, Jacobsen AJ, Torrents A et al (2011) Ultralightmetallic microlattices. Science 334(6058):962–965. https://doi.org/10.1126/science.1211649

[50] Lu TJ, Stone HA, Ashby MF (1998) Heat transfer in open-cell metal foams. Acta Materialia 46(10):3619–3635. https://doi.org/ 10.1016/S1359-6454(98)00031-7

[51] Catchpole-Smith S, Sélo RR, Davis AW, et al (2019) Thermal conductivity of TPMS lattice structures manufactured via laser powder bed fusion. Additive Manufacturing 30(August):100,846. https://doi.org/10.1016/j.addma.2019.100846

[52] Goransson P (2006) Acoustic and vibrational damping in porous solids. Philosophical Transactions of the Royal Society A: Mathematical, Physical and Engineering Sciences 364(1838):89–108. https://doi.org/10.1098/RSTA.2005.1688

[53] Brown JA, Bishop JE, Brennan-Craddock J, et al (2012) The design of impact absorbing structures for additive manufacture. Journal of Physics: Conference Series 382(012042). https://doi.org/10.1088/1742-6596/382/1/012042

[54] McConaha M, Anand S (2020) Design of stochastic lattice structures for additive manufacturing. International Manufacturing Science and Engineering Conference 1:1–11. https://doi.org/10. 1115/MSEC2020-8439

[55] Groth JH, Anderson C, Magnini M et al (2022) Five simple tools for stochastic lattice creation. Additive Manufacturing 49(102):488. https://doi.org/10.1016/J.ADDMA.2021.102488

[56] Maliaris G, Sarafis E (2016) Mechanical behavior of 3D printed stochastic lattice structures. Solid State Phenomena 258:225–228. https://doi.org/10.4028/www.scientific.net/SSP.258.225

[57] Ashby MF, Evans AG, Fleck NA, et al (2000) Metal foams: a design guide. Butterworth-Heinemann, Woburn, http://www.bh.com

[58] Martínez J, Song H, Dumas J, et al (2017) Orthotropic k-nearest foams for additive manufacturing. ACM Trans Graph 36(4). https://doi.org/10.1145/3072959.3073638ï, https://hal.archives-ouvertes. fr/hal-01577859

[59] Goguelin S (2022) 3D printing in orthopedics: better knee, hip & spine implants. https://all3dp.com/1/3d-printing-orthopedicsknee-hip-spine-implants/

[60] Kondjoyan A, Péneau F, Boisson HC (2002) Effect of high free stream turbulence on heat transfer between plates and air flows: a review of existing experimental results. Int J Ther Sci 41(1):1–16. https://doi.org/10.1016/S1290-0729(01)01299-.www.sciencedirect.com/science/article/pii/S1290072901012996

[61] Choy SY, Sun CN, Leong KF et al (2017) Compressive properties of functionally graded lattice structures manufactured by selective laser melting. Mater Des 131:112–120. https://doi.org/10.1016/J.MATDES.2017.06.006

[62] Mukhopadhyay T, Adhikari S (2017) Effective in-plane elastic moduli of quasi-random spatially irregular hexagonal lattices. Int J Eng Sci 119:142–179. https://doi.org/10.1016/J.IJENGSCI.2017. 06.004

[63] Yin H, Huang X, Scarpa F et al (2018) In-plane crashworthiness of bio-inspired hierarchical honeycombs. Composite Structures 192:516–527. https://doi.org/10.1016/J.COMPSTRUCT.2018.03. 050

[64] Gen3D (2021) Sulis V1.9.10 65. Develop3D (2022) Gen3D rolls out Sulis V1.10. https://develop3d. com/cad/gen3d-rolls-out-sulis-v1-10/

[65] Mathworks Inc. (2020) MATLAB 2020b 67. Synopsys (2021) Simpleware ScanIP v2021

[66] Dassault-Systems (2020) ABAQUS v2020

[67] Jahns K, Bappert R, Böhlke P et al (2020) Additive manufacturing of CuCr1Zr by development of a gas atomization and laser powder bed fusion routine. Int J Adv Manuf Technol 107(5–6):2151–2161. https://doi.org/10.1007/s00170-020-04941-7

[68] Du Y, Mukherjee T, Finch N et al (2022) High-throughput screening of surface roughness during additive manufacturing. J Manuf Process 81(June):65–77. https://doi.org/10.1016/j.jmapro.2022.06.049

[69] Sharma, K. (2023). Innovative Applications of AI, Machine Learning, and Smart Technologies in Non destructive Testing (NDT). e-Journal of Nondestructive Testing. Vol. 28(10). https://doi.org/10.58286/28706

[70] Sharma, K. (2023). Innovative Applications of AI, Machine Learning, and Smart Technologies in Non destructive Testing (NDT). e-Journal of Nondestructive Testing. Vol. 28(10). https://doi.org/10.58286/28706

Licensed Under Creative Commons Attribution CC BY